

Article

Numerical Simulation Study on the Damage Mechanism of the Combined Perforating Well Testing Tubing in Ultra-Deep Wells

Jiadong Jiang ^{1,2,3}, Qiao Deng ^{1,2,3,*}, Dong Yang ^{1,2,3,*}, Guilin Qi ^{1,2,3}, Fan Zhang ⁴ and Leichuan Tan ⁵

¹ Cooperative Innovation Center of Unconventional Oil and Gas, Yangtze University, Wuhan 430100, China; jjd720473@163.com (J.J.); qigulin1024@163.com (G.Q.)

² Hubei Key Laboratory of Oil and Gas Drilling and Production Engineering, Yangtze University, Wuhan 430100, China

³ National Engineering Research Center for Oil & Gas Drilling and Completion Technology, School of Petroleum Engineering, Yangtze University, Wuhan 430100, China

⁴ CNPC Chuanqing Drilling Engineering Company Limited, International Engineering Company, Chengdu 610051, China; zhangfan18120@163.com

⁵ CNPC Chuanqing Drilling Engineering Company Limited, Chengdu 610051, China; tanleichuan0220@126.com

* Correspondence: dengqiao@yangtzeu.edu.cn (Q.D.); 521005@yangtzeu.edu.cn (D.Y.)

Abstract: During perforation in ultra-deep wells, the blast shock wave can induce dynamic responses of the perforating tubing, leading to potential downhole accidents such as vibration, deformation, and even fracture of the perforating tubing. To comprehend the dynamic response characteristics of the perforating tubing under blast impact load, we conducted a joint finite element simulation using SolidWorks, Hypermesh, and LS-DYNA. The simulation included deformation analysis, motion analysis, and strength analysis of the perforating tubing. By analyzing these factors, we obtained the change in velocity, acceleration, and equivalent stress of the perforating tubing over time under the blast load. The finite element analysis indicates the following: (a) the bottom of the perforating tubing is susceptible to significant tension compression cycle; (b) the velocity amplitude variation is smallest at the top of the perforating tubing, while the frequency and peak values of velocity changes are maximal at the bottom of the perforating tubing; and (c) the top and bottom of the tubing string are the vulnerable parts of the perforating tubing system.

Keywords: petroleum perforation; perforating tubing; ultra-deep well; shock wave; dynamics analysis; effective stress; numerical simulation; damage mechanism



Citation: Jiang, J.; Deng, Q.; Yang, D.; Qi, G.; Zhang, F.; Tan, L. Numerical Simulation Study on the Damage Mechanism of the Combined Perforating Well Testing Tubing in Ultra-Deep Wells. *Processes* **2024**, *12*, 380. <https://doi.org/10.3390/pr12020380>

Academic Editor: Qingbang Meng

Received: 9 January 2024

Revised: 23 January 2024

Accepted: 24 January 2024

Published: 14 February 2024



Copyright: © 2024 by the authors. Licensee MDPI, Basel, Switzerland. This article is an open access article distributed under the terms and conditions of the Creative Commons Attribution (CC BY) license (<https://creativecommons.org/licenses/by/4.0/>).

1. Introduction

Perforation refers to the utilization of specialized instruments, typically, perforating guns, to detonate charges. This process enables the charges to penetrate the casing and cement sheath, creating channels (as shown in Figure 1). These channels, established between the reservoir and the wellbore, facilitate the flow of reservoir fluids into the wellbore, promoting the routine production of oil and gas wells.

Existing perforating processes include tubing-conveyed perforating (TCP) and wireline-conveyed perforating (CCP), which are widely used because tubing-conveyed perforating can carry out deep penetration operations. And with the development of perforating technology, a single perforating process has been developed into a perforating–testing–acidizing process. In this process, the perforating gun is connected with testing instruments to form an integrated tubing, which enables a single tubing to simultaneously perform perforating, well killing, fluid drainage, etc., thereby reducing the frequency of tubing retrieval and deployment and, consequently, lowering the cost of well testing [1–4].

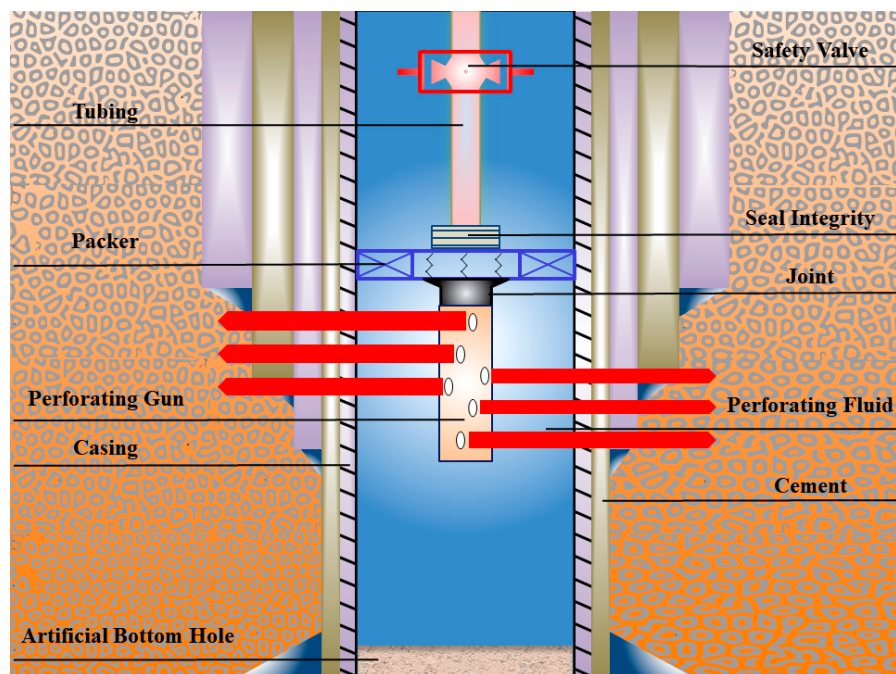


Figure 1. Schematic diagram of perforating operation.

Simultaneously, in the pursuit of further enhancing oil and gas production, many oilfield construction organizations have implemented high perforating density and lengthened perforating gun design [5,6], which increases the impact pressure generated by the perforating operation, making the perforating tubing more susceptible to buckling and fracture. Once the perforating tubing string in the wellbore fails and falls into the well, it becomes an obstacle, hindering operations such as fracturing and testing and posing risks to the daily production of oil and gas wells.

Numerous issues arising from perforating tubing incidents in China have been documented, including stuck pipe, debris and cuttings, formation damage, pressure and fluid loss, as well as tool failure [7–12] (as shown in Figure 2). For instance, during the testing and perforating of tubing in the Keshen-101 well and Wushen-1 well in the Tarim Oilfield in western China, the tubing below the packer fractured, resulting in its descent into the well. Similarly, there have been instances of tubing buckling and fracturing due to excessive pressure generated by the blast from perforation [13]. A notable case is the Manati-1 well in the Camamu Basin of Brazil, where the pulsating pressure generated by the perforation blast led to the shear failure of the ignition head, causing the tubing to fall into the well [14].



Figure 2. Plastic bending of perforating tubing string [12].

Perforation, as a specialized technological process, faces a complex downhole environment in oil and gas wells, involving diverse interdisciplinary knowledge such as underwater explosions, tubing dynamics, and shock wave propagation. Consequently, transferring methods and theories from other fields to directly address the trials encountered in perforation becomes a significant challenge. In the domain of underwater explosions, many scholars have focused on the response of metallic structures. For instance, in 2007, John, M. B. et al. investigated the dynamic response of a cylindrical shell underwater to shock waves and bubble pulsation by extracting acceleration and pressure data, employing high-speed imaging techniques [15]. In 2014, Bowen, X. et al. used AUTODYN and ABAQUS to study the dynamic response of a cylindrical shell in water under the impact load of three types of explosives [16]. In 2020, Kevin, B. et al. studied the deformation patterns of a cylindrical shell in different water depths through mathematical modeling and LS-DYNA finite element simulations [17]. In 2023, Weizheng, X. et al. conducted a photonic experiment on the dynamic response of a cylindrical shell structure under explosive loading in a water tank [18]. However, these studies primarily focused on cylindrical shells in open-water environments (as shown in Figure 3), where the propagation of underwater shock waves is relatively straightforward.

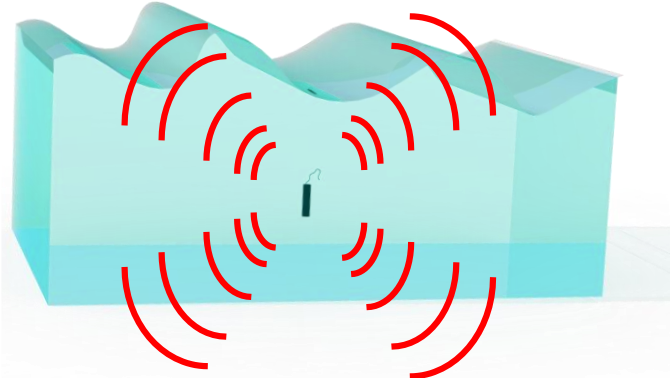


Figure 3. Schematic of an underwater explosion in open water.

Perforation operations, on the other hand, are conducted in the confined and elongated downhole environment of the well's sealed section in. The propagation process of shock waves during perforation is intricate and involves continuous reflection and coupling within the casing. Therefore, though research on damage to cylindrical shells in open-water explosion is valuable, there are challenges in direct research on damage to perforating tubing in the complex downhole environment.

In the domain of perforating tubing mechanics, various studies have been conducted to analyze different aspects. In 2003, Hongdong, Y. et al. performed a mechanical analysis of the longitudinal vibration of a perforating testing tubing, highlighting that the primary influencing factor on tubing vibration is the high pressure generated during perforation operation [10]. In 2011, Jack, B. et al. discussed a computer modeling program addressing the safety of perforating tubing, aiming to assess the mechanical risks faced by perforating tubing inside the wellbore [19]. In 2012, Yihua, D. et al. conducted a study comparing data from different wells to investigate the impact of parameters such as perforation interval, wellbore bottom, and perforation ratio on the strength of perforating tubing string [20]. In 2019, Mingfei, L. et al. studied the dynamic response of tubing by establishing a dynamic theory model and using ANSYS [21]. In 2023, Jun, L. et al. explored the vibration characteristics of tubing under different construction parameters [22]. However, these studies have tended to overlook the complex operating conditions of perforating tubing string, specifically in the high-temperature and high-pressure conditions of ultra-deep wells. This lack of consideration has resulted in an incomplete and non-systematic understanding of the mechanisms causing damage to perforating tubing, making the resolution of tubing impact safety issues challenging.

Due to the multidisciplinary nature of perforation technology, conducting large-scale perforating experiments is impractical. Moreover, perforating tubing string in ultra-deep wells faces complex conditions such as high temperature and high pressure, contributing to a lack of accurate and systematic recognition of the perforating tubing damage mechanism. The challenge of addressing tubing safety issues remains difficult. Utilizing numerical simulation, a widely applied computer technology in engineering [23,24], allows for the comprehensive simulation and calculation of the entire perforation process.

In this paper, we used numerical simulation to establish a finite element model and analyzed the simulation and results. The perforating tubing system is modeled by SolidWorks based on the actual engineering parameters of an oil and gas well in southwestern China, the meshing is conducted by Hypermesh, and the boundary conditions, equations of state, and data solving are set by LS-DYNA. In this paper, we extracted the data of displacement, velocity, acceleration, and equivalent stress of the tubing to reveal the vulnerable links of the perforating tubing system and explored the risks faced by the tubing during the perforating operation. Meanwhile, we plotted pressure contour plots to demonstrate the propagation of the blast wave in the perforating fluid and the perforating gun. Finally, the accuracy of the numerical simulation is demonstrated by example verification.

2. Materials and Methods

2.1. Simulation Modeling

The perforating tubing system comprises various downhole devices, such as manometers and negative pressure valves. To streamline computations and provide a more intuitive exploration of the impact of the perforation blast load on the perforating tubing, the perforating tubing string system is simplified. Using a straight 7660 m ultra-deep well in the southwest oilfield of China as a representative case, the three-dimensional model is constructed using SolidWorks. This model, depicted in Figure 4, incorporates components such as the charge, perforating gun, casing, perforating fluid, tubing, and connectors, based on actual parameters.

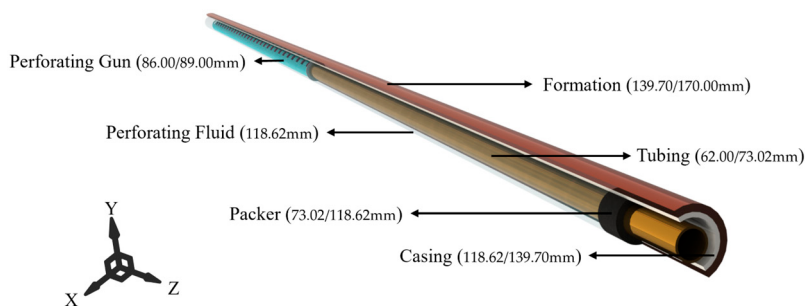


Figure 4. Schematic diagram of the model of the perforating tubing system.

The perforation operation parameters include an initial wellbore pressure of 99.19 MPa, the setting depth of the packer at 7197 m, 2656 perforation charges, each with an explosive of 25 g, and the perforating fluid density of 1320 kg/m^3 . Among these, the perforating gun is made of 32CrMo4 steel, and the tubing and casing are of N80 steel grade. Specific modeling parameters, as per API [25], are detailed in Table 1.

2.2. Algorithm, Material, and Boundary Condition Setting

The established perforating tubing system model is imported into Hypermesh for the meshing of each component, ensuring that the Jacobian of 2D mesh quality is within the range of 0.6 to 1. Finally, the 2D mesh is mapped to a 3D eight-node hexahedral solid element (as shown in Figure 5). The Lagrange algorithm, which facilitates the determination of material boundary movement and provides accurate results for small deformations [26], is a commonly used finite element analysis method for studying solid structures. Therefore, the mesh models for the perforating gun, tubing, and casing are established using the

Lagrange algorithm. The ALE algorithm combines the advantages of Lagrange and Euler algorithms. In solving the grid calculation, each step can have an arbitrary motion relative to the coordinate system, avoiding the problem of insufficient accuracy caused by the direct calculation of large deformation grids [27]. Hence, the explosive and perforating fluid utilizes the ALE algorithm to establish mesh models. Simultaneously, owing to the highly nonlinear nature of perforation explosions, the explosive region undergoes mesh refinement, as depicted in Figure 6.

Table 1. Parameters of the main model components of the perforating system.

Components	Length (m)	Density ($\text{kg} \cdot \text{m}^{-3}$)	Size (mm)	Yield Strength (MPa)	Modulus of Elasticity (GPa)	Poisson's Ratio
Perforating Fluid	Tubing	226	7800	62.00/73.02	536	206
	Casing	463	7800	118.62/139.70	460	206
	Packer	0.1	1975	73.02/118.62	/	0.49
	Formation	462	1320	118.62	/	/
	Perforating Gun	463	2620	139.70/170.00	/	66
		166	7800	86.00/89.00	550	206

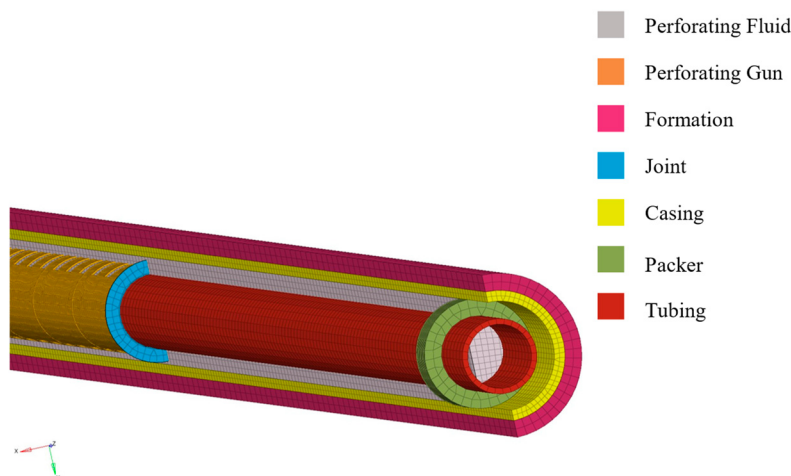


Figure 5. Partial view of the grid model of the perforating tubing string system.

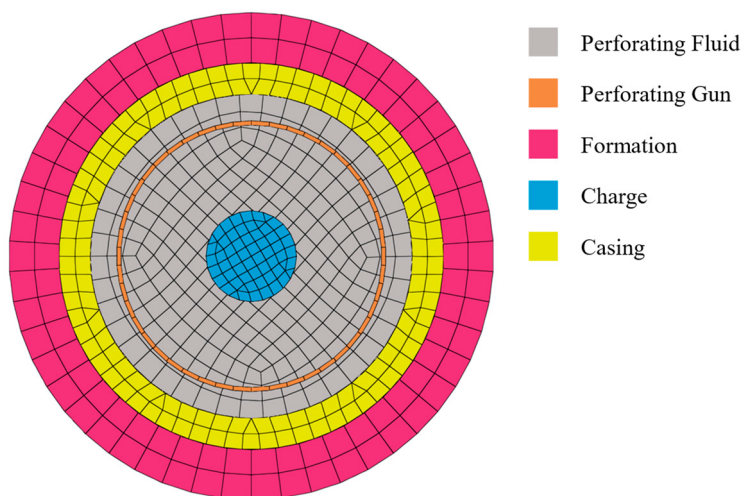


Figure 6. Cross-section view of the mesh model.

Before setting the boundary conditions, the perforating tubing string is taken as the research subject. In relation to the buoyancy, gravity, perforation impact force exerted on the tubing downhole, and the characteristics of perforation operations in the sealed section

of ultra-deep wells, the following assumptions are made for the finite element model of the perforating tubing system.

1. The initial position of the tubing aligns with the borehole axis of the oil and gas well;
2. The tubing is treated as an elastic material and its material exhibits isotropic properties;
3. The gravitational force acting on the tubing due to downhole components is disregarded.

In accordance with the aforementioned assumptions, boundary conditions are set in LS-DYNA. Initially, upon detonation of the charges, the resulting shock wave propagates above the perforating tubing. Considering that the inner wall of the casing functions as a rigid surface, the shock wave predominantly undergoes continuous reflection within the casing. When the shock wave propagates upward to the packer, due to the rubber material of the packer, it results in more shock wave ground transmitting out at the interface between the packer and the perforating fluid. Consequently, a non-reflective boundary condition is applied at this interface.

Due to the perforating fluid being in an ultra-deep well environment, the pressure applied to the perforating tubing cannot be overlooked. Therefore, an equivalent pressure load is applied to the perforating fluid to simulate the effect of gravity on the fluid and an external load is applied to the outer surface of the casing to simulate soil-casing interaction. Due to the differing propagation characteristics of shock waves in rigid compared to elastic material, and considering the packer is made of rubber, the casing is assumed to be rigid. Finally, contact settings between components in contact within the wellbore are established on SURFACE-TO-SURFACE in LS-DYNA.

The perforating blast is a chemical reaction process that spans tens to hundreds of milliseconds [28]. The ZND model is acknowledged as suitable for describing the explosion process and elucidating the chemical reaction of explosives that generate high temperatures and pressures by means of a pre-pressurized shock wave. Upon completion of the reaction, it delineates the final state of the blast. This model aligns well with the phenomenon of the perforating gun's perforating blast. Consequently, we establish the ZND model's ignition to generate the explosives' perforating charge in LS-DYNA.

The explosive in the perforating charge is HMX, designated as the HIGH_EXPLOSIVE_BURN material model in LS-DYNA. To illustrate the expansion work process of the perforating blast products within the high-temperature and high-pressure gas mass, the Jones–Wilkins–Lee equation of state (JWL) [29] is employed. This equation accurately captures the pressure-density energy characteristics of the detonation products and can be expressed as follows:

$$P_w = A_1 \left(1 - \frac{\omega_1}{R_1 V_w} \right) e^{-R_1 V_w} + A_2 \left(1 - \frac{\omega_1}{R_2 V_w} \right) e^{-R_2 V_w} + \frac{\omega_1 E_w}{V_w} \quad (1)$$

where P_w is the explosive blast pressure; V_w is the relative volume; E_w is the unit volume of explosive initial explosion internal energy; and A_1 , A_2 , R_1 , R_2 , and ω_1 are the equation of state constants. The parameters of the JWL equation of state for the HMX charge are shown in Table 2.

Table 2. The parameters of HMX explosives for charges.

Density (g·cm ⁻³)	Explosive Velocity (cm·μs ⁻¹)	A_1 (GPa)	A_2 (GPa)	R_1	R_2	ω_1	E_w (kJ·cm ⁻³)
1.89	0.91	778.3	7.07	4.2	0.99	0.3	0.105

The perforating fluid material adopts the MAT_NULL model and, simultaneously, the Grüneisen state equation is applied to it:

$$p = \frac{\rho_0 C^2 \mu [1 + (1 - \frac{\gamma_0}{2})\mu - \frac{a}{2}\mu^2]}{\left[1 - (S_1 - 1) - S_2 \frac{\mu^2}{\mu+1} - S_3 \frac{\mu^3}{(\mu+1)^2}\right]} + (\gamma_0 + a\mu)E \quad (2)$$

where ρ_0 is the material's initial density; C is the intercept of the shock wave velocity curve; μ is the medium's compression coefficient; a is the first-order volume correction coefficient of γ_0 ; S_1 , S_2 , and S_3 are the slope coefficients of the material's stress wave velocity curve; γ_0 is the gamma coefficient of the Grüneisen state equation; and E is the internal energy per unit initial volume. The parameters of the Grüneisen state equation for the perforating fluid are shown in Table 3.

Table 3. The parameters of the Grüneisen state equation for the perforating fluid.

Density (g·cm ⁻³)	C (m·s ⁻¹)	μ (N·s·m ⁻²)	a	S_1	S_2	S_3	γ_0	E (Pa)
1.00	1.647×10^3	0.8684×10^{-3}	0	1.921	-0.096	0	0.35	2.895×10^5

3. Results and Discussion

3.1. Deformation Analysis of Perforating Tubing

After parameters settings, we introduced additional pre-processing steps into the perforating tubing string system. These steps involve defining boundary conditions, specifying contact conditions, and applying loads, all aimed at simulating perforating shock wave transmission and reflection to the fullest extent. Subsequently, stress contour plots are examined and kinetic data from the pre-processing setup are extracted upon completion of the simulation solution. Using the unit system of mm-g-μs, contour plots illustrating the combined displacement changes of the perforating tubing at different moments are generated to observe the dynamic response process, as depicted in Figure 7.

During the perforating operation, the generated blast load impacts the perforating tubing for a very brief period, causing a significant pressure surge [30]. This surge results from the blast gas pressure within the perforating gun, the formation pore pressure, and the wellbore fluid pressure [31]. Consequently, the perforating tubing undergoes displacement due to the instantaneous impact of the generated blast wave. As illustrated in Figure 7, at 0 μs, i.e., before the start of the perforating operation, the perforating blast wave was not generated and the tubing was not displaced. After the detonation of the charge, the bottom of the tubing closest to the explosion area exhibits the initial response with displacement and deformation. At 1500 μs, the perforating tubing unit block progressively displaces from the bottom to the top due to the bottom-up propagation of the shock load generated by the charge explosion. At 5000 μs, as the top of the perforating tubing is distanced from the explosion area, the perforating tubing itself can absorb a certain amount of blast energy [32]. Additionally, the packer restrains the top of the tubing, resulting in the least displacement and deformation at the top and the greatest displacement and deformation at the bottom of the tubing.

To gain a clearer understanding of the tubing's deformation pattern in all directions, displacement-time data in the X, Y, and Z directions are extracted from any node at the bottom of the tubing, as depicted in Figure 8. Following the detonation of the charge, the bottom of the tubing experiences different degrees of displacement changes in the X, Y, and Z directions. Due to the constraining of the casing, the radial displacement changes generated by unidirectional shear deformation in the X and Y directions is small. In contrast, the Z direction at the bottom of the tubing, due to the lack of external restraint, exhibits more obvious impact-induced deformation under the burst load and, thus, is susceptible to fatigue damage.

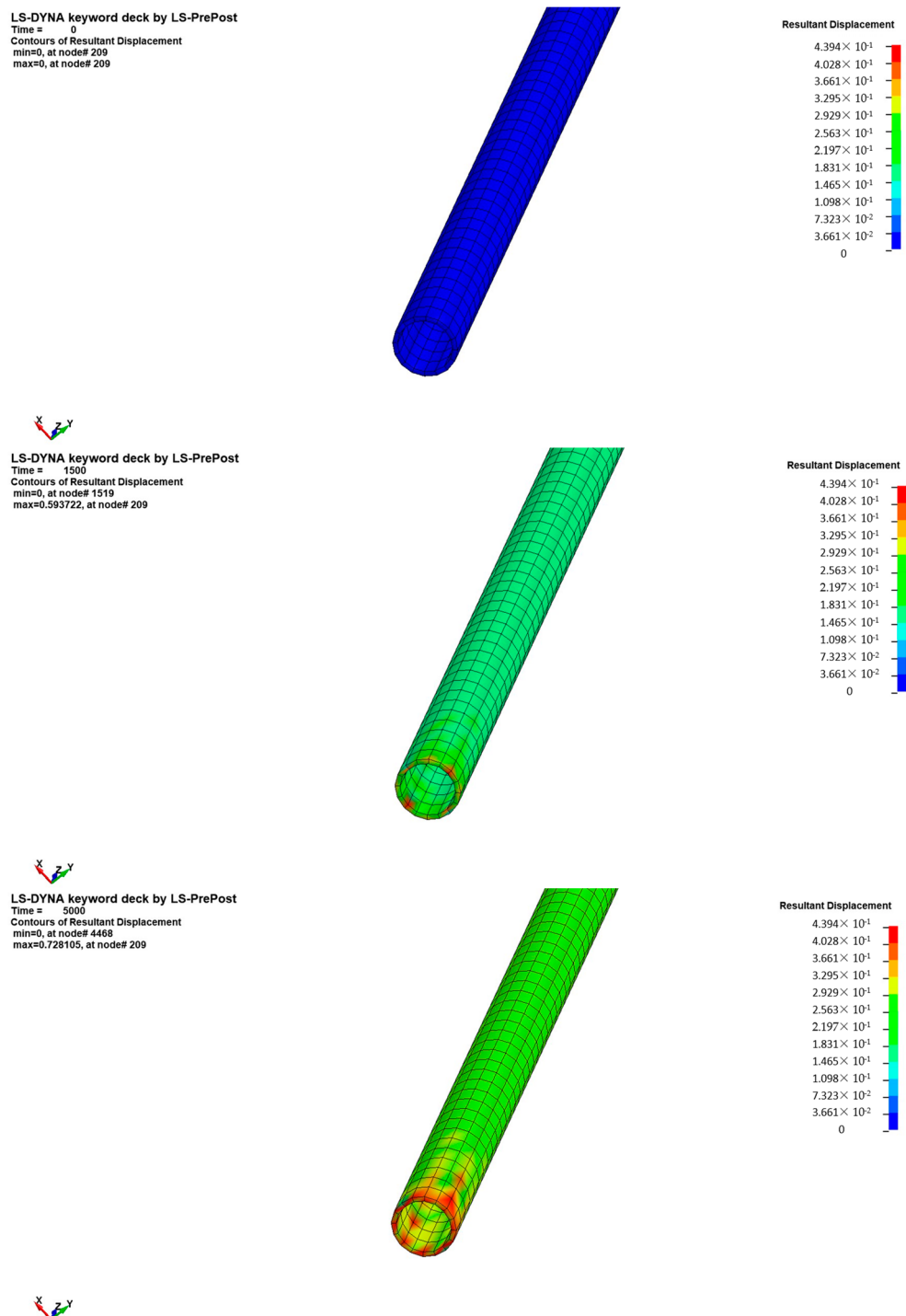


Figure 7. The variation of displacement of the bottom of the perforating tubing at different moments, respectively, 0 μ s, 1500 μ s, and 5000 μ s.

Between 450 μ s and 700 μ s, the bottom of the tubing rebounded in the X, Y, and Z directions. This rebound is attributed to the simplification of the charge as a cylindrical explosive in the modeling. The detonation of explosives does not instantaneously complete the chemical reaction but progressively concludes it. With explosives positioned at a certain spatial distance from the top and bottom of the tubing, the detonation wave rebounds at the top and bottom, resulting in the observed rebound at the bottom of the tubing. As the rebound transmits to the bottom of the tubing, a retraction in displacement occurs. Next, 700 μ s later, the chemical reaction within the explosives accelerates, producing more

blast waves that counteract part of the initial rebound. Simultaneously, the tubing stores elastic energy and kinetic energy from the blast [33], contributing to a gradual increase in displacement at the bottom of the perforating tubing string.

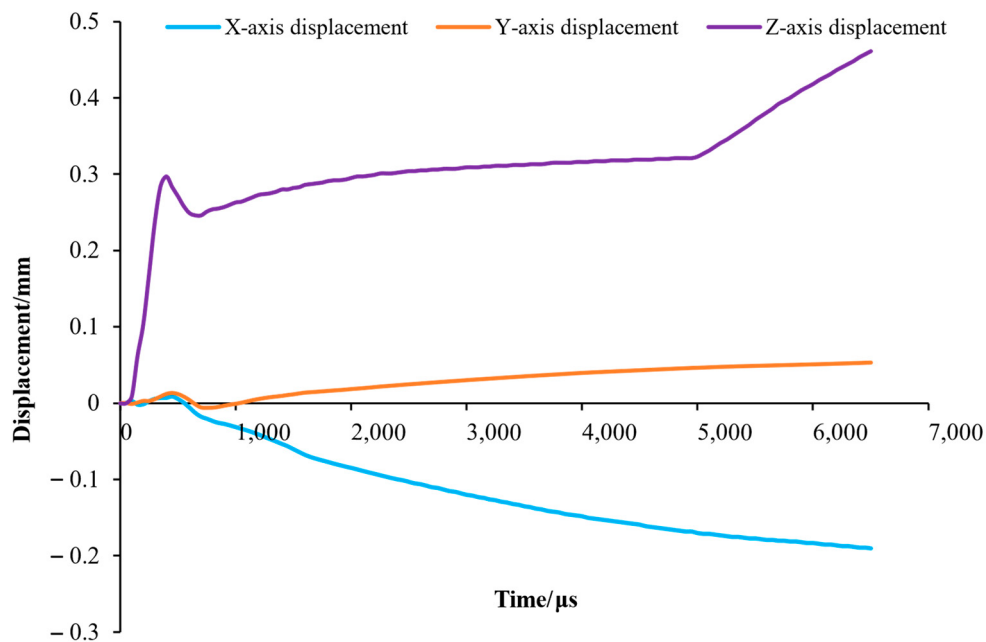


Figure 8. Displacement variations in three directions at the bottom of the perforating tubing string.

3.2. Movement Analysis of Perforating Tubing

Figure 9 illustrates the three-directional acceleration-time curves for a unit block at the bottom of the perforating tubing in the X, Y, and Z directions. It can be seen from the figure that the acceleration of the tubing exhibits fluctuations and oscillations in the X, Y, and Z directions, with acceleration values gradually decreasing and stabilizing over time. This can be attributed to the transient explosion of the charge, resulting in a substantial perforating impact load propagated upward by the perforating gun. Simultaneously, the detonation wave undergoes reflection and refraction on the rigid surfaces of the casing and tubing, leading to energy decay in the blast wave over time [34].

Considering that the Z-axis direction of the perforating tubing string is only constrained by the top packer, while the bottom of the Z-axis remains unconstrained, the peak acceleration in the Z-axis is notably greater than that in the X and Y directions. The X and Y directions, which are constrained by the casing, contribute to the differences in peak accelerations.

To comprehend the motion velocity of different sections of the perforating tubing, motion data are extracted from the top, middle, and bottom of the tubing. As depicted in Figure 10, around 100 μ s, the top and bottom of the perforating tubing nearly reached their peak velocities, with the central part attaining its peak velocity later. The peak velocity of the central part falls between that of the top and bottom sections. During the outward expansion of the explosive gas generated by the charges, it propels the perforating fluid upward. When the expansion halts, the upward-moving perforating fluid, under gravity, returns to compress the explosive gas, resulting in increased pressure [21]. This process induces pulsation changes at the bottom of the perforating tubing.

In terms of the magnitude of velocity fluctuations, the top of the tubing exhibits the smallest changes. It is evident that the bottom of the perforating tubing linked to the perforating gun is subject to the initial impact of the blast wave, leading to intense velocity oscillations at the bottom. Moreover, since it takes time for the upward propagation of the blast wave and tubing and casing absorb some blast wave energy, there is a significant

energy decay during the wave propagation. The top of the tubing constrained by the packer mitigates the velocity fluctuations at its upper end to some extent.

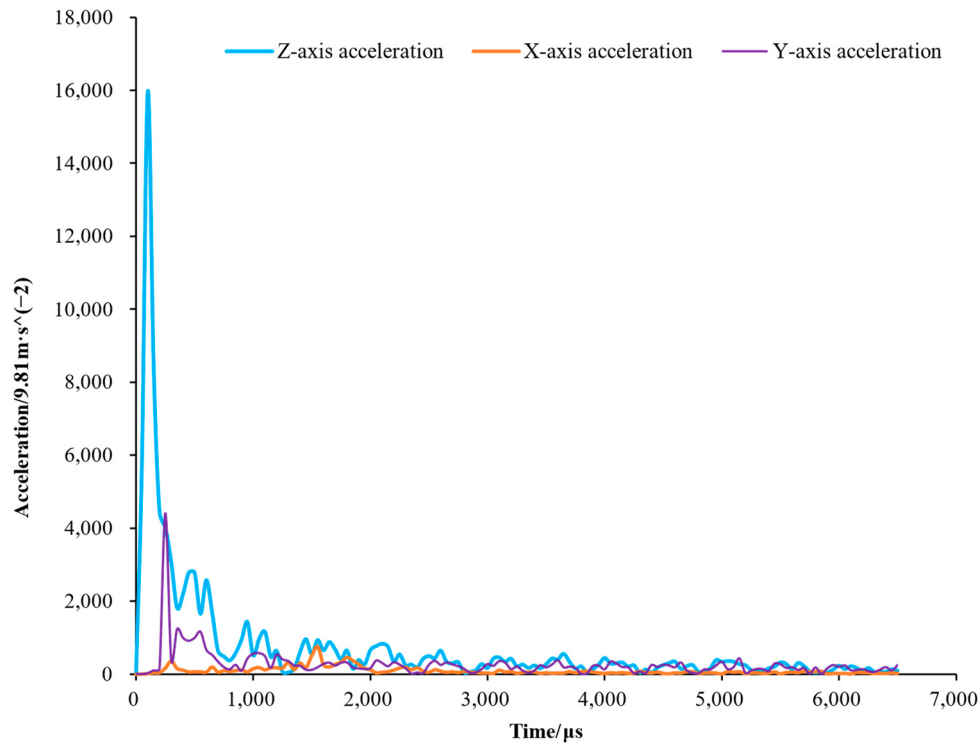


Figure 9. Variation of acceleration in three directions at the bottom of the perforating tubing at different moments.

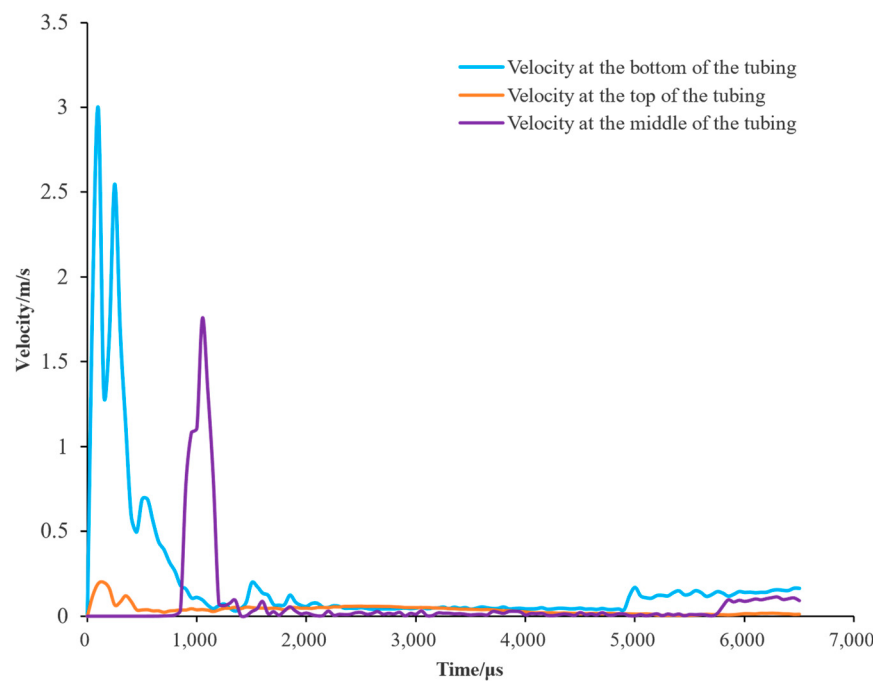


Figure 10. Velocity changes at the top, middle, and bottom of the tubing at different moments.

3.3. Strength Analysis of Perforating Tubing

After analysis of motion and deformation in the perforating tubing, the dynamic response characteristics become evident. Figure 11 shows the contour plots of equivalent

stress in the perforating tubing at each moment after the detonation of the charges measured in units of 100 MPa. Through an analysis of Figure 11, it is evident we must consider how the strength of the perforating tubing string changes with time under the influence of the perforating blast load.

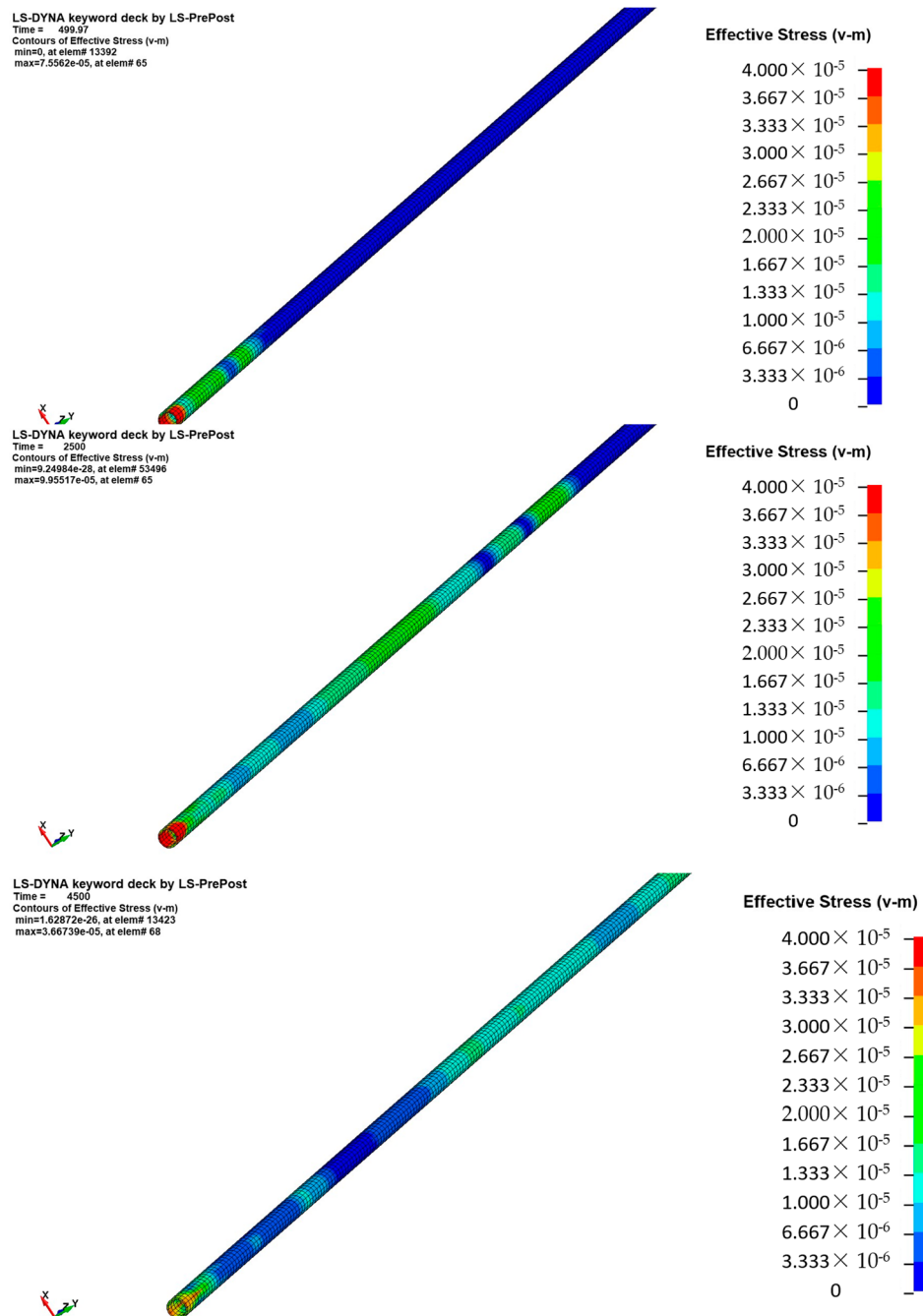


Figure 11. Equivalent stress distribution of perforating tubing at different moments, at, respectively, 300 μ s, 2000 μ s, and 6500 μ s.

At 300 μ s, the explosive detonates, generating perforation impact load that acts on the bottom of the tubing, leading to the concentration of local equivalent stress. By 2000 μ s, the response at the top of the tubing, constrained by the packer fixation due to the upward propagation of the blast wave, initiates, causing a gradual rise in equivalent stress at the top. Subsequently, at 6500 μ s, the blast wave commences reflecting from the top to the bottom, concentrating the equivalent stress in a local area of the tubing.

To further investigate the kinetic response pattern of the overall equivalent stress in the perforating tubing, we extracted the equivalent stress data over time for corresponding unit blocks at the top, middle, and bottom of the tubing. As depicted in Figure 12, despite the brief explosion duration and the rapid speed of the blast wave, the propagation of the explosive shock wave still takes some time. Consequently, the impact load on each part of the tubing does not react simultaneously but sequentially.

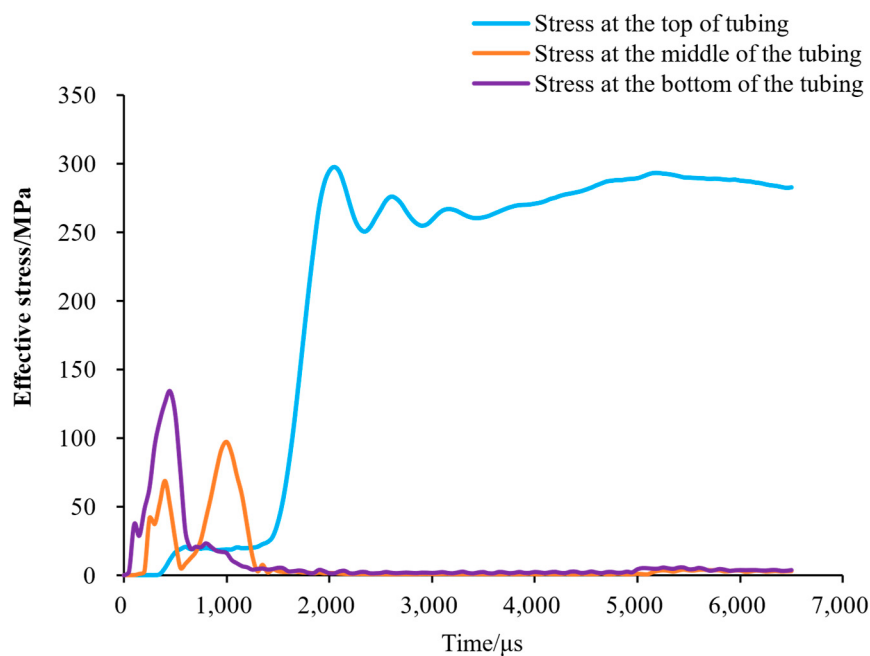


Figure 12. The variation of equivalent stress of perforating tubing at different moments.

Upon detonation of the explosive, the bottom of the tubing initially experienced a peak equivalent stress of 134.09 MPa. With the upward propagation of the blast wave, the middle of the tubing exhibited a peak stress of 97.16 MPa, while the top registered a peak equivalent stress of 293.83 MPa. Notably, the three sections of the perforating tubing do not immediately decay with time after reaching their respective peaks but react again to the tubing after the blast wave reflects at the bottom of the well, causing the three parts of the tubing to generate equivalent stress peaks once more.

Subsequently, the downward rebound of the blast wave from the packer, coupled with the upward reflection of the blast wave from the bottom of the well, can be regarded as the next cycle of change. According to the Von Mises yield criterion, if the maximum equivalent stress at the top of the perforating tubing exceeds the yield value of the tubing material itself due to the tensile–compressive stresses generated during downhole perforating operations, the perforating tubing will yield [35]. This indicates that the top of the perforating tubing is a vulnerable link in the overall system. In subsequent studies, the Von Mises stress equivalence criterion can also be applied to predict the vibration fatigue life of the vulnerable part of the tubing.

3.4. Propagation of Blast Wave

To further investigate the propagation of blast waves in perforating fluid, we extracted pressure from the perforating fluid inside the wellbore during the perforation process and plotted a pressure distribution contour plot. Figure 13 illustrates how the explosion caused by the detonation of the charges causes a high-temperature, high-pressure gas to expand and compress the perforating fluid, increasing fluid pressure and driving the movement of the fluid. At 500 μ s, the blast wave propagates upward, reaching the interface with the packer. Owing to the packer's restriction, some blast waves reflect downward. A contour plot similar to this one was generated in order to analyze the blast wave propagation within

the perforating gun. Since the perforating gun is near the bottom of the well, the blast wave goes upward to the well bottom and causes a pressure response in the perforating gun that is similar to that of perforating fluid (as shown in Figure 14).

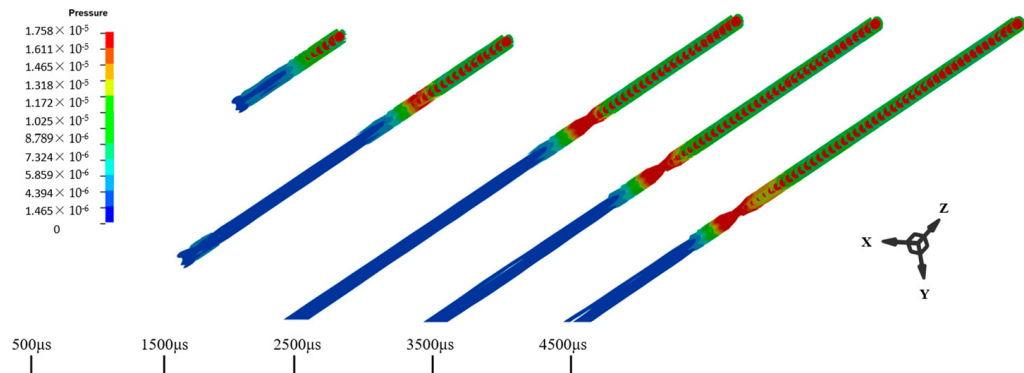


Figure 13. Propagation of blast waves in the perforating fluid.

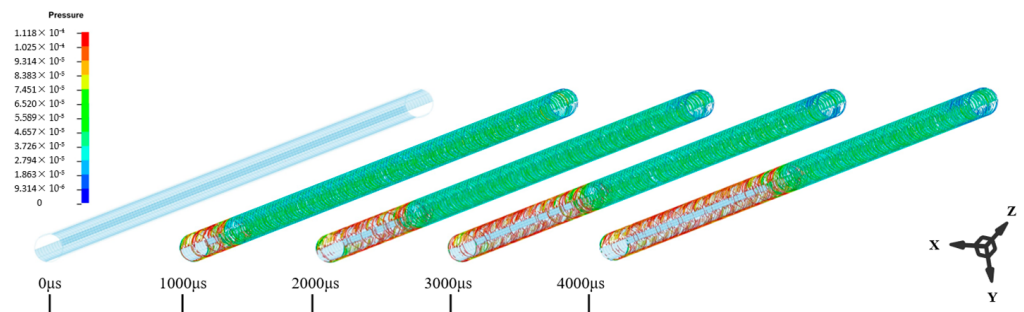


Figure 14. Propagation of blast waves in the perforating gun.

3.5. Validation

To validate the accuracy of the numerical simulation model, we extracted the displacement data for the tubing. It is observed that during the perforating tubing operation, the blast wave generated by the charges explosion induced dynamic responses in the tubing, resulting in changes in tubing displacement. Simultaneously, the tubing's displacement alteration increased over time, eventually leading to a fracture at the top of the tubing, as depicted in Figure 15. Furthermore, as shown in Figure 16, the fracture position of the perforating tubing was discovered to be near the top of the tubing in the majority of field wells. This observation lends some support to the correctness of the numerical simulation.

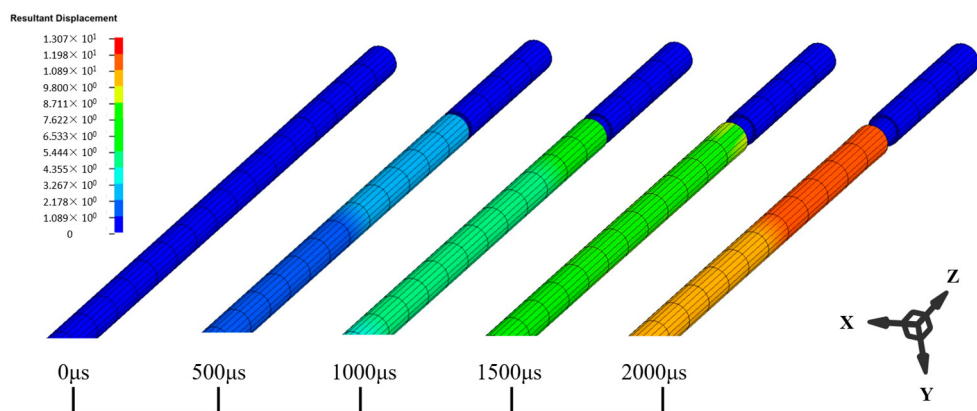


Figure 15. Resultant displacement of the top of the perforating string.



Figure 16. Fracture failure of the perforating tubing string [12].

The numerical simulation model parameters in this paper are derived from the structural parameters of the well and the actual perforating operation parameters of an oil and gas well in southwestern China. It is worth noting that the perforating tubing of this well experienced fracture during the field perforating operation. The ultimate tensile force leading to fracture for the perforating tubing used in the oil field site is measured at 530 kN. In contrast, the peak axial force in the numerical simulation model reaches approximately 460 kN, as depicted in Figure 17. The margin of error between the two values is about 13.2%, demonstrating that the accuracy of this numerical simulation falls within a reasonable engineering margin of error.

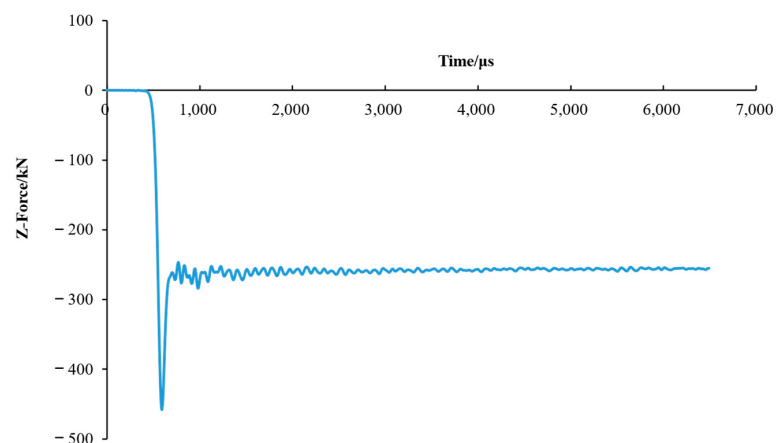


Figure 17. Axial force of perforating tubing.

4. Conclusions

This paper conducts a collaborative simulation to investigate the dynamic response characteristics of the perforating tubing string during downhole perforating operations in ultra-deep wells. The study covers tubing deformation, tubing motion, and tubing strength, deriving the response laws of the perforating tubing string. The analysis leads to the following conclusions:

- (a) The perforating impact load induces a significant pressure step for the perforating tubing string, leading to an overall displacement of the perforating tubing. As the tubing itself absorbs a portion of the energy transmitted by the shock wave during propagation and considering the top of the tubing is farther away from the explosion center, the deformation of the top of the tubing is comparatively smaller. In contrast, the displacement deformation at the bottom of the tubing is more pronounced. The velocity–time curve of the perforating tubing reveals that the bottom of the tubing

- experiences the fastest velocity changes within the perforating tubing string system. Additionally, the unconstrained Z-axis direction at the bottom of the tubing exhibits a noticeably higher peak acceleration than in other directions, indicating that the bottom of the tubing is highly susceptible to deformation in the perforating tubing system;
- (b) Following the volatile explosion, the shock wave affects the bottom, center, and top of the perforating tubing over time, resulting in these sections' respective peak equivalent stresses. The shock wave undergoes rebound transmission between the top of the packer and the bottom of the well, causing fluctuations in the equivalent stress of the perforating tubing, characterized by peaks and subsequent decay. Notably, due to the largest peak equivalent stress occurring at the top of the tubing, the Von Mises yield criterion suggests that the top of the tubing is particularly susceptible to fatigue damage within the entire system;
- (c) To accurately and systematically analyze the dynamic mechanical response of tubing during perforating tubing operations, numerical simulation can serve as a valuable tool for studying the safety aspects of perforating tubing under various working conditions. In instances where simulations indicate incidents like tubing fractures, adjustments can be made to pertinent process parameters during the perforating process. For example, reducing the number of perforating charges can help mitigate the impact load from the perforating blast and adjusting the perforating fluid density can reduce the initial pressure exerted on the perforating tubing, among other potential adjustments.

Author Contributions: Writing—review and editing, J.J. and Q.D.; conceptualization, D.Y.; formal analysis, G.Q.; methodology, F.Z. and L.T. All authors have read and agreed to the published version of the manuscript.

Funding: This study was supported by the Key Program of the Hubei Provincial Department of Education, no. D20221303; the Natural Science Foundation of Hubei Province, no. 2022CFB700; the Open Fund of the Hubei Key Laboratory of Drilling and Production Engineering for Oil and Gas (Yangtze University), no. YQZC202206; and the Open Foundation of Cooperative Innovation Center of Unconventional Oil and Gas, Yangtze University (Ministry of Education & Hubei Province), no. UOG2024-06.

Data Availability Statement: Data are contained within the article.

Conflicts of Interest: Author Fan Zhang was employed by the company CNPC Chuanqing Drilling Engineering Company Limited, International Engineering Company. Author Leichuan Tan was employed by the company CNPC Chuanqing Drilling Engineering Company Limited. The remaining authors declare that the research was conducted in the absence of any commercial or financial relationships that could be construed as a potential conflict of interest.

Abbreviation

TCP	tubing-conveyed perforating
WCP	wireline-conveyed perforating
mm	millimeter
cm	centimeter
m	meter
Pa	Pascal
MPa	million Pascal
GPa	giga Pascal
g	gram
kg	kilogram
μs	microsecond
s	second
kJ	kilo-Joule
N	Newton
kN	kilo-Newton

References

- Shoujun, W.; Zhongjian, T.; Xiaojiang, H.; Bing, X.; Zhenjiang, L.; Weihua, F. An offshore combination technology of composite perforation and formation testing and its application. *China Offshore Oil Gas* **2013**, *25*, 8–12.
- Chengwu, G.; Jiewen, S.; Qiang, Z.; Yanwu, W.; Jianfeng, Z. Application of testing technology in complex gas reservoirs of A-mu Darya. *Oil Drill. Prod. Technol.* **2014**, *36*, 126–128.
- Fei, L.; Ronghe, L. New development of combined process of perforating-acidizing-testing technology. *Drill. Prod. Technol.* **2016**, *39*, 79–82.
- Yong, Y.; Zhitong, S.; Xianbin, L.; Xuedong, F.; Wei, X.; Jingun, L. Research and application of dynamic negative pressure perforation acidification and test combination technology in high temperature, high pressure and low permeability reservoir of Qinghai oilfield. *Drill. Prod. Technol.* **2020**, *43*, 129–131.
- Jim, G.; Derek, B.; Rajani, S.; Crystal, L.; Jesse, H.; Baker, H. The Importance of Pre-Job Shock Modeling as a Risk Mitigation Tool in TCP Operations. In Proceedings of the SPE Deepwater Drilling and Completions Conference, Galveston, TX, USA, 10–11 September 2014.
- Sharif, A.; Andy, M.; Angel, U.; Javier, M.C. Wireline-Deployed Perforating: Maximizing Efficiency without Killing the Well. In Proceedings of the SPE/ICoTA Coiled Tubing and Well Intervention Conference and Exhibition, Houston, TX, USA, 21–22 March 2017.
- Kai, T.; Haidong, W.; Jianxin, P.; Huabing, C.; Miaozhuang, L.; Jianbo, C.; Chuangang, D. Perforating technology for super high temperature and pressure 8000 m deep wells. *Drill. Prod. Technol.* **2018**, *41*, 57–60.
- Zifeng, L. Research advances and debates on tubular mechanics in oil and gas wells. *Acta Pet. Sin.* **2016**, *37*, 531–556.
- Yihua, D.; Xiaodong, Z.; Yongjun, F.; Mingfei, L. Fluid-solid interaction analysis for perforation gun jamming and strength considering effects of blasting height and phase angle. *J. Vib. Shock* **2022**, *41*, 167–173.
- Hongdong, Y.; Shiyi, L.; Jianjun, Z. Mechanics analysis of perforating combined well testing string and protection technology of downhole instrument. *Oil Drill. Prod. Technol.* **2003**, *03*, 61–63+85.
- Mingfei, L.; Fei, X.; Yihua, D. Dynamic response analysis of a perforated pipe string under detonation impact load. *J. Vib. Shock* **2019**, *38*, 185–191+222.
- Qiao, D. Safety Analysis for Downhole Wellbore during Perforating. Ph.D. Thesis, China University of Petroleum (Beijing), Beijing, China, 2020.
- Yihua, D.; Haijun, X.; Xuehai, J.; Dongming, Z. Analysis of the cause of damage to the center tube of the perforating combined well testing packer. *China Pet. Mach.* **2007**, *343*, 113–115.
- Canal, C.; Priscilla, M.; Scott, M.; Jovineto, M.; Darren, B. Predicting Pressure Behavior and Dynamic Shock Loads on Completion Hardware during Perforating. In Proceedings of the 2010 Offshore Technology Conference, Houston, TX, USA, 3–6 May 2010.
- John, M.B.; George, Y. A study of explosive effects in close proximity to a submerged cylinder. *Int. J. Impact Eng.* **2008**, *35*, 206–225.
- Bowen, X.; Yajie, W.; Guoning, R.; Jinhua, P. Dynamic Response of Underwater Cylindrical Shells Subjected to Blast Loads of Aluminized Explosives. *Explos. Mater.* **2014**, *43*, 1–5.
- Kevin, B.; Herve, L.S.; Guillaume, B. Estimation of the response of a deeply immersed cylinder to the shock wave generated by an underwater explosion. *Mar. Struct.* **2020**, *72*, 1–22.
- Weizheng, X.; Hongtao, Z.; Yexun, L.; Yu, H.; Hua, F. An experimental study on dynamic response of cylindrical shell under near-field/contact underwater explosion. *Explos. Shock Waves* **2023**, *43*, 209–219.
- Jack, B.; Martin, S.; Cam, L.; David, S. Predicting Wellbore Dynamic-Shock Loads Prior to Perforating. In Proceedings of the SPE Digital Energy Conference and Exhibition, Woodlands, TX, USA, 19–21 April 2011.
- Yihua, D.; Mingfei, L.; Fuxiang, Z.; Xiangtong, Y. An analysis of the effect of the well bore structure on the strength safety of the tubing string at the perforation section. *China Pet. Mach.* **2012**, *40*, 27–29.
- Mingfei, L.; Fei, X.; Yihua, D. Measurement of perforating column vibration parameters and ALE-based numerical simulation. *Chin. J. Appl. Mech.* **2019**, *36*, 458–465+515.
- Jun, L.; Yilin, J.; Yili, C.; Kai, T.; Guohui, R.; Jianbo, C. Shock vibration response characteristic of perforating tubing string in ultra-deep wells. *Geoenergy Sci. Eng.* **2023**, *228*, 1–23.
- Carlos, B.; Keith, B.; Lu, A.; Harvey, W.; Fuxiang, Z.; Xiangtong, Y.; Jianxin, P. Prediction and Reduction of Perforating Gunshock Loads. In Proceedings of the International Petroleum Technology Conference, Beijing, China, 26–28 March 2013.
- Carlos, B.; Angel, L.; Paulo, V.; Harvey, W.; Paulo, S. Perforating Gunshock Loads—Prediction and Mitigation. In Proceedings of the SPE/IA-DC Drilling Conference and Exhibition, Amsterdam, The Netherlands, 5–7 March 2013.
- API. *Technical Report on Equations and Calculations for Casing, Tubing and Line Pipe Used as Casing or Tubing; and Performance Properties Tables for Casing and Tubing*, TR 5C3; API: Washington, DC, USA, 2008.
- Xin, G.; Qing, Z. Progress in numerical simulation of dam failure under blast loading. *J. Hohai Univ. (Nat. Sci.)* **2017**, *45*, 45–55.
- Guanghong, M.; Yu, H.; Jiuying, A.; Qiuyue, M.; Zhihao, S.; Honghao, M.; Zhaowu, S. Numerical simulation of explosive welding of metal tube and rod based on different algorithms. *Trans. China Weld. Inst.* **2022**, *43*, 64–71+116–117.
- Xi, L.; Shushan, W.; Feng, M.; Haifeng, Z. Dynamic responses test of perforating string section under explosion Impact. *Sci. Technol. Eng.* **2014**, *14*, 53–56+92.
- Xingyu, Z.; Chunhua, B.; Jian, Y.; Bingfeng, S. Parameters calculation of JWL EOS of FAE detonation products. *Acta Armamentarii* **2020**, *41*, 1921–1929.

30. Wei, Z.; Cheng, X.; Mingfei, L.; Lin, Z.; Gangqin, W. Transient response and strength analysis of perforating string. *China Pet. Mach.* **2017**, *45*, 90–94+110.
31. Carlos, B.; Denny, G.; Alan, S.; Moises, S.; Indah, P.; Risal, R.; Sandy, W. Perforating on Wireline: Maximizing Productivity and Minimizing Gunshock. In Proceedings of the SPE European Formation Damage Conference and Exhibition, Budapest, Hungary, 3–5 June 2015.
32. William, S.; Carlos, B.; Harvey, W.; Flavio, M.; Jonathan, S.; Martin, B.; Scott, O. Efficient Perforation of High-Pressure Deepwater Wells. In Proceedings of the Offshore Technology Conference, Houston, TX, USA, 2–5 May 2011.
33. Mark, B.; Andrea, B.; Carlos, B. Perforating Gunshock Loads: Simulation Capabilities and Applications. In Proceedings of the International Petroleum Technology Conference, Kuala Lumpur, Malaysia, 10–12 December 2014.
34. Qiao, D.; Hui, Z.; Jun, L.; Hao, W.; Xuejun, H. Safety Distances of Packers for Deep-Water Tubing-Conveyed Perforating. In Proceedings of the Offshore Technology Conference, Houston, TX, USA, 30 April–3 May 2018.
35. Zifeng, L. Applicability of unified strength theory in tubular mechanics and safety stress field of the material with SD effect. *Acta Pet. Sin.* **2016**, *37*, 1537–1542.

Disclaimer/Publisher's Note: The statements, opinions and data contained in all publications are solely those of the individual author(s) and contributor(s) and not of MDPI and/or the editor(s). MDPI and/or the editor(s) disclaim responsibility for any injury to people or property resulting from any ideas, methods, instructions or products referred to in the content.